

# Violation of Bell's inequality for phase singular beams

Shashi Prabhakar,\* Salla Gangi Reddy, A Aadhi, Chithrabhanu P, G. K. Samanta, and R. P. Singh  
*Physical Research Laboratory, Navrangpura, Ahmedabad. 380009, India.*

(Dated: May 17, 2022)

We have experimentally verified the violation of Bell's inequality for continuous variables of position and momentum for beams with phase singularities. Given that Wigner distribution function (WDF) provides information about position and momentum simultaneously, it has been used to derive Bell's inequality for phase singular beams [Phys. Rev. A **88**, 013830 (2013)]. We have measured the WDF taking recourse to Fourier transform of the two point correlation function for vortex beams.

PACS numbers: 42.50.Tx, 42.25.Kb, 03.65.Ud

Optical vortices, phase singularities of the field, are observed as dark spots in bright background. Being topological structures, they are robust and find applications in free space [1] and fiber communication [2]. For the vortex of topological charge  $n$ , the azimuthal phase variation is  $2\pi n$  in a full rotation around the dark spot [3]. The sense of rotation of phase provides the sign of its charge. The topological charge  $n$  can be considered as an important parameter for such beams. One of the main characteristics of these beams is that they carry an orbital angular momentum (OAM) of  $n\hbar$  per photon [4]. The OAM carrying property has raised extensive interest in scientific community due to its unique applications in the fields of particle manipulation [5] and quantum information [6–8]. Vortex beams have been experimentally realized both in lasers [9] as well as electron beams [10, 11]. These beams form an infinite dimensional basis for applications such as quantum computation and cryptography [6, 12]. Moreover, increase in information entropy with the order of vortices can be utilised to encode more amount of information in these structures [13, 14].

Study of the Wigner distribution function (WDF) for classical beams has been found to be very useful since it can provide coherence information in terms of the joint position and momentum (phase-space) distribution for a particular optical field [15, 16]. Recently, the famous Bell's inequality has been defined for classical sources using the WDF and it has been shown theoretically that the optical vortex beams violate this inequality [17]. This indicates existence of quantum like entanglement between continuous variables of position and momentum. Such quantum inspired inseparability has been termed as "classical entanglement" [18, 19].

In this article, we have demonstrated the experimental verification of "classical entanglement" using the WDF and two-point Bell's inequality for optical vortex beams [17]. We produce different orders of vortex beams using a spatial light modulator (SLM) [20] and obtained two-point correlation function using interference between vortices of the same order in a shearing Sagnac interferometer (SSI) [21, 22].

The electric field of an optical vortex of order  $n$  and

centered at origin can be written in terms of Laguerre Gaussian (LG) modes

$$E_{nm}(r, \phi, z) = \frac{C_{nm}^{LG}}{w(z)} \left( \frac{r\sqrt{2}}{w(z)} \right)^{|n|} \exp\left(-\frac{r^2}{w^2(z)}\right) \times L_m^{|n|} \left( \frac{2r^2}{w^2(z)} \right) \exp\left(ik\frac{r^2}{2R(z)}\right) \exp(in\phi) \times \exp[i(2m + |n| + 1)\zeta(z)], \quad (1)$$

where  $L_m^{|n|}$  is the generalized Laguerre polynomial, the radial index  $m > 0$  and the azimuthal index is  $n$ .  $C_{nm}^{LG}$  is the normalization constant,  $w(z)$ ,  $R(z)$  and  $\zeta(z)$  are beam parameters and  $r$ ,  $\phi$  are radial and azimuthal coordinates in space respectively. Such beams contain azimuthal phase dependence of  $\exp(in\phi)$  and singularity at the center.

The WDF for optical vortex beams can be written as [15, 23]

$$W_{nm}(X, P_X; Y, P_Y) = \frac{(-1)^{n+m}}{\pi^2} L_n[4(Q_0 + Q_2)] \times L_m[4(Q_0 - Q_2)] \exp(-4Q_0), \quad (2)$$

where  $\{X, P_X\}$  and  $\{Y, P_Y\}$  are conjugate pairs of dimensionless quadratures while  $Q_0$  and  $Q_2$  are

$$Q_0 = \frac{1}{4} [X^2 + P_X^2 + Y^2 + P_Y^2], \\ Q_2 = \frac{XP_Y - YP_X}{2}. \quad (3)$$

The scaled variables  $X$ ,  $P_X$ ,  $Y$  and  $P_Y$  can be defined as

$$x(y) \rightarrow \frac{w}{\sqrt{2}} X(Y), \\ p_x(p_y) \rightarrow \frac{\sqrt{2}\lambda}{w} P_X(P_Y) \quad (4)$$

and follow  $[\widehat{X}, \widehat{P}_X] = [\widehat{Y}, \widehat{P}_Y] = i$ .

The WDF defined in Eq. 2 can be obtained by taking the Fourier transform (FT) of two-point correlation function (TPCF) that is defined as

$$\Phi(x, \epsilon_x; y, \epsilon_y) = \langle E(\epsilon_x + x/2, \epsilon_y + y/2) \times E^*(\epsilon_x - x/2, \epsilon_y - y/2) \rangle, \quad (5)$$

In fact, in experiment one measures TPCF only, to determine the WDF.

For discrete entangled systems, the Bell-CHSH inequality can be written as [24, 25]

$$B = |S(a, b) + S(a, b') + S(a', b) - S(a', b')| < 2, \quad (6)$$

where  $(a, b)$ ,  $(a', b')$  are two analyser settings and  $S(a, b)$  is the joint probability corresponding to settings  $(a, b)$ . The entanglement in quantum systems with continuous variables is characterized by probabilities. For continuous variable systems, WDF is expressed as an expectation value of a product of displaced parity operators. Banaszek and Wodkiewicz [26, 27] have argued that the WDF can be used to derive the analog of Bell's inequality in continuous variable systems.

Considering the transformation  $\Pi(X, P_X; Y, P_Y) = \pi^2 W(X, P_X; Y, P_Y)$  in dimensionless quadratures, the Bell-CHSH inequality  $B$  with chosen points  $\{a, b\} \equiv \{X1, P_{X1}; Y1, P_{Y1}\}$  and  $\{a', b'\} \equiv \{X2, P_{X2}; Y2, P_{Y2}\}$  can be written as

$$B = \Pi_{nm}(X1, P_{X1}; Y1, P_{Y1}) + \Pi_{nm}(X1, P_{X1}; Y2, P_{Y2}) \\ + \Pi_{nm}(X2, P_{X2}; Y1, P_{Y1}) \\ - \Pi_{nm}(X2, P_{X2}; Y2, P_{Y2}) < 2. \quad (7)$$

From Eq. 2, the WDF of an optical vortex beam with topological charge  $n = 1$  can be obtained as

$$W_{10}(X, P_X; Y, P_Y) = e^{-X^2 - P_X^2 - Y^2 - P_Y^2} \times \\ \frac{(P_X - Y)^2 + (P_Y + X)^2 - 1}{\pi^2}. \quad (8)$$

Choosing  $X1 = 0, P_{X1} = 0, X2 = X, P_{X2} = 0, Y1 = 0, P_{Y1} = 0, Y2 = 0, P_{Y2} = P_Y$ , the Bell-CHSH parameter can be written as

$$B = \Pi_{10}(0, 0; 0, 0) + \Pi_{10}(X, 0; 0, 0) \\ + \Pi_{10}(0, 0; 0, P_Y) - \Pi_{10}(X, 0; 0, P_Y) \quad (9)$$

$$= e^{-P_Y^2} (P_Y^2 - 1) + e^{-X^2} (X^2 - 1) - \\ e^{-P_Y^2 - X^2} [(P_Y + X)^2 - 1] - 1. \quad (10)$$

The maximum Bell's violation considering only two variables  $X$  and  $P_Y$  is  $|B_{max}| \sim 2.17$  which occurs at  $X \sim 0.45$  and  $P_Y \sim 0.45$ . Considering all eight variables from Eq. 7, the maximum Bell's violation is  $|B_{max}| \sim 2.24$  at  $X1 \sim -0.07, P_{X1} \sim 0.05, X2 \sim 0.4, P_{X2} \sim -0.26, Y1 \sim -0.05, P_{Y1} \sim -0.07, Y2 \sim 0.26$  and  $P_{Y2} \sim 0.4$ .

The experimental setup to find the TPCF is shown in Fig. 1. Computer generated holography has been used to generate optical vortices [28]. A Gaussian laser beam from an intensity stabilized He-Ne laser (Spectra-Physics, 117A) is incident normally to the SLM (Holoeye, LC-R 2500) using the mirror M1 and the beam splitter BS1. The SLM is a liquid-crystal-based device that can modulate light and can be used as a dynamic diffractive optical

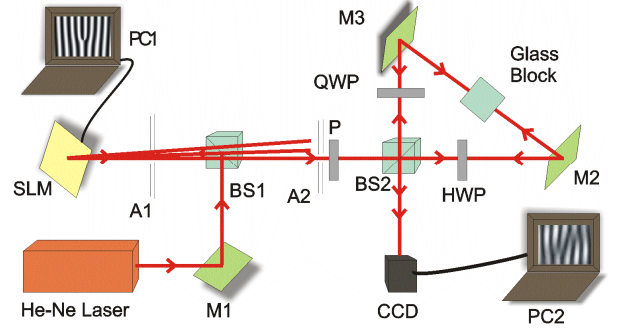


FIG. 1. (Color online) Experimental setup for determination of TPCF.

element. Vortices of different orders are produced in the first diffracted order by introducing different fork patterns onto the SLM via a computer PC1. Apertures A1 and A2 are used to select an optical vortex of the desired order. A polarizer (P) is used to fix the polarization of the optical vortex. The vortex with the vertical polarization is coupled to the Shearing-Sagnac interferometer (SSI) that comprises the beam splitter BS2 and two mirrors, M2 and M3. A quarter-wave plate (QWP) and a half-wave plate (HWP) are kept in common path for the quadrature selection. A glass block mounted upon a rotation stage is also kept in the common path to introduce the shear in two transverse directions. This arrangement ensures that both the clockwise (CW) and the counter-clockwise (CCW) fields experience one reflection from and one transmission through the beam splitter. This removes the effect of deviations from 50% transmission and polarization-sensitivity of the beam splitters. The two counter-propagating beams are interfered and imaged using a Evolution VF cooled CCD camera that is connected to computer PC2.

First, we have calibrated the shear in laser-beam produced by the glass block. For this, we put one polarizer inside the SSI. The CW and CCW propagation of beams were chosen by rotation of the polarizer. We have used regular grating on the SLM to propagate Gaussian beam inside the SSI to maintain uniformity of experimental condition. Starting with a zero shear, we provide gradual shear to the beam using glass block mounted on a rotation stage with linear scale. The shear is varied in equal steps. A particular tilt to the glass block will produce the shear in the beams propagating inside the SSI. We have recorded the intensity of two beams with CCD camera. These images were processed in Matlab to determine the shear between the two beams. The beam width  $w$  of the Gaussian laser beam falling on the CCD was determined using the 2D curve-fitting in Matlab. The scaled shear was obtained using Eq. 4 corresponding to the linear scale on rotation stage of the glass block. We have achieved the required shears after calibrating the

SSI. The amount of shear as a function of linear scale of the rotation stage has been shown in Fig. 2.

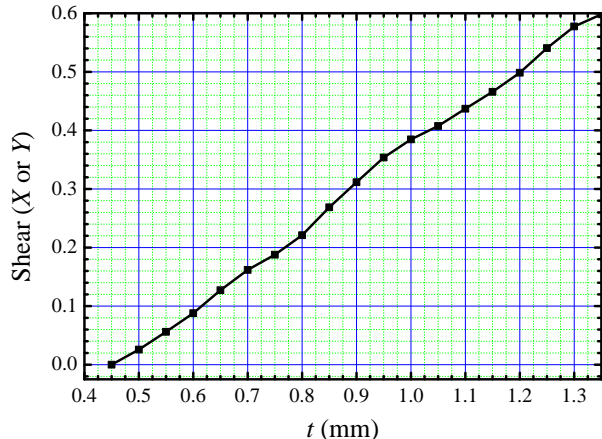


FIG. 2. (Color online) Calibration curve for dimensionless shear ( $X, Y$ ) in the SSI. The  $x$ -axis ( $t$ ) denotes the position on linear scale present on the mount on which the cube was mounted.

The main part of our experiment is to determine the TPCF [13, 21]. For various tilt of the glass block, we have recorded the interferograms by keeping the fast axes of the QWP and the HWP parallel to the incident beams' polarization direction. In this orientation, the wave plates have no effect on the polarization of the optical beam, and both the CW and CCW propagating fields travel equal optical path lengths inside the SSI. The recorded interferograms contain the information of  $\text{Re}[\Phi(X, \epsilon_x; Y, \epsilon_y)]$ . Measurement of  $\text{Im}[\Phi(X, \epsilon_x; Y, \epsilon_y)]$  is achieved by rotating HWP by  $\pi/4$ , resulting in a  $3\pi/4$  optical delay between the counter-propagating fields. Keeping the same lateral shear values, another set of interferograms are recorded which contain the  $\text{Im}[\Phi(X, \epsilon_x; Y, \epsilon_y)]$ . Fig. 3(a) and 3(b) show the TPCF of Gaussian beam and optical vortex of topological charge  $n=1$  respectively. These TPCFs are obtained at zero shears ( $X=0, Y=0$ ). To obtain the TPCF at different shears ( $X, Y$ ), the glass cube is rotated to corresponding positions along  $x$  and  $y$  axes suggested by Fig. 2.

To obtain the WDF, we have taken the FT of TPCF [15]. Fig. 3(c) shows the WDF of an optical vortex with topological charge  $n=1$  and  $m=0$  obtained at  $X=Y=0$ , corresponding TPCF is shown in Fig. 3(b). This shows that our results are consistent with the previously obtained WDFs [15]. After obtaining four WDFs at chosen shear values ( $X1, Y1$ ), ( $X2, Y1$ ), ( $X1, Y2$ ) and ( $X2, Y2$ ), the four dimensional addition was performed over  $P_{X1}, P_{X2}, P_{Y1}, P_{Y2}$  axes to determine  $B$  as defined in Eq. 7. The experimentally obtained WDF is a two-dimensional ( $P_X, P_Y$ ) function, keeping two dimensions ( $X, Y$ ) to be constant. However, after addition of four WDFs, the dimension for  $B$  is a four-dimensional func-

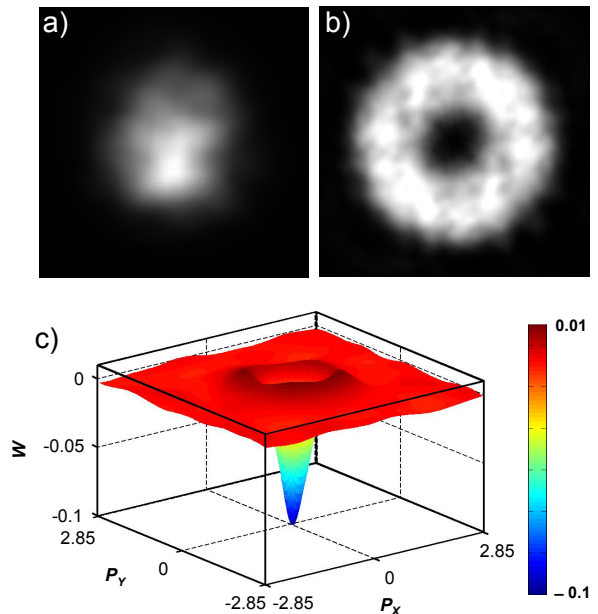


FIG. 3. (Color online) Experimentally obtained a) TPCF for Gaussian beam, b) TPCF and c) WDF for optical vortex of topological charge  $n=1, m=0$  and shears  $X=Y=0$ .

tion ( $P_{X1}, P_{X2}, P_{Y1}, P_{Y2}$ ) while other four dimensions ( $X1, X2, Y1, Y2$ ) are fixed. Equation 7 shows the generation of a four-dimensional matrix after adding four two-dimensional functions. Proper axes should be considered while adding. The maximum value of  $B$  was determined to verify the violation of Bell's inequality.

Considering  $X1=0, P_{X1}=0, X2=X, P_{X2}=0, Y1=0, P_{Y1}=0, Y2=0, P_{Y2}=P_Y$ , the 2D surface plot of  $|B|$  varying with  $X$  and  $P_Y$  described by Eq. 9 is shown in Fig. 4. From the plot, location of the maximum of  $|B|$  has been determined that matches with the theory. The  $|B_{max}|$  obtained from Fig. 4 is 2.1793, which indicates that the continuous variables of optical vortex field are non-separable.

The data points in Fig. 4 show some scatter since the vortices have been generated through diffraction from the SLM. One may see the experimental results of intensity correlations for different order of vortices formed using SLM vis-à-vis a Gaussian laser beam for a comparison [29]. The small fluctuations in Fig. 4 can be attributed to the finite number of data points while recording TPCF experimentally and discrete Fast Fourier transform of that data while determining WDF.

Corresponding to vortices of order  $n=1, 2$  and  $3$  as well as for the Gaussian ( $n=0$ ), Eq. 7 has been used to obtain values of  $X1, X2, Y1, Y2$  which will maximize  $B$ . These parameter values have been used to select the desired shear in the experimental measurements of the TPCF, which provides us the WDF through Fourier transform. The obtained parameters are listed in Table I.

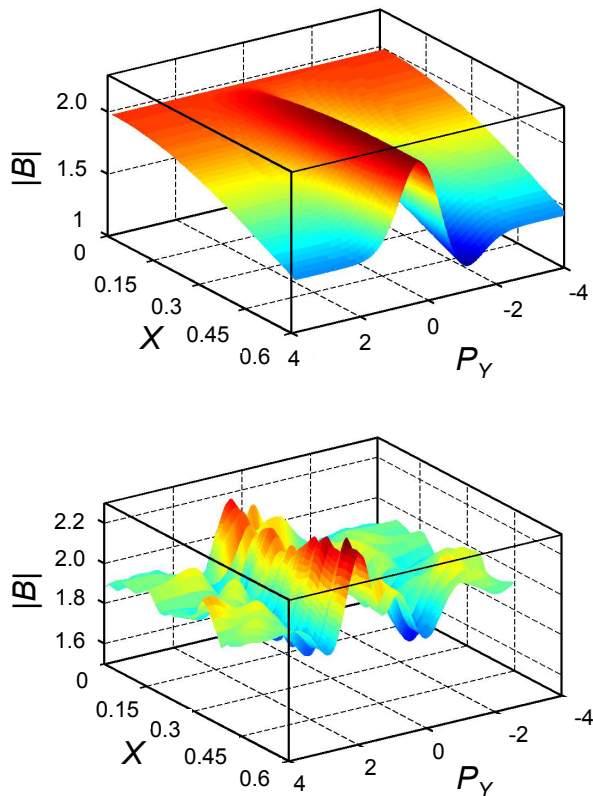


FIG. 4. (Color online) Variation of  $|B|$  with  $X$  and  $P_Y$  (Eq. 9) for  $n = 1$  and  $m = 0$ . Theoretical (top) and experimental (bottom) for  $X1=0$ ,  $P_{X1}=0$ ,  $X2=X$ ,  $P_{X2}=0$ ,  $Y1=0$ ,  $P_{Y1}=0$ ,  $Y2=0$  and  $P_{Y2} = P_Y$ .

$n$	$ B_{max} $	$(X1, X2, Y1, Y2)$
0	2.00	(0.00, 0.58, 0.00, 0.00)
1	2.24	(-0.07, 0.40, -0.05, 0.26)
2	2.35	(0.09, -0.40, 0.00, 0.00)
3	2.40	(-0.09, 0.35, -0.01, 0.06)

TABLE I. Theoretical values of variables providing  $|B_{max}|$ .

Figure 5 shows the variation of maximum Bell's inequality violation ( $|B_{max}|$ ) for a Gaussian beam ( $n = m = 0$ ) and the optical vortices of order  $n = 1-3$ ,  $m = 0$ . From Fig. 5, it is clear that there is no Bell's inequality violation for the Gaussian beam. However, for the optical vortex beams, the Bell's inequality has been violated. The amount of Bell's violation increases with the increase in order of the vortices. The amount of entanglement increases with the order of an optical vortex due to the increase in Bell's violation parameter ( $B_{max}$ ). Since, the earlier results also point out an increase in information entropy [13], a measure of entanglement, with the order of vortex, therefore, in the present case,  $|B_{max}|$  can be used to obtain the degree of entanglement. We have also performed experiments around the point of  $|B_{max}|$  and

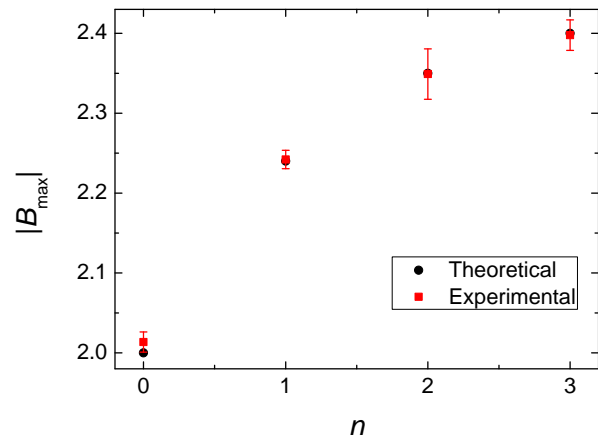


FIG. 5. (Color online) Variation of  $|B_{max}|$  with the order of vortex ( $n$ ) and  $m = 0$  obtained at parameters mentioned in Table I.

observed that amount of Bell's violation decreases as we move away from the point of maxima.

To estimate the experimental error, the experiment was repeated for five times. In every set of experiment, four WDFs were determined and for each WDF, two sets of inteferograms corresponding to real and imaginary component of TPCF were recorded.  $|B_{max}|$  was calculated for each set of experiments. The  $|B_{max}|$  used in Fig. 5 is the average of five  $|B_{max}|$  determined from each set of experimental inteferograms. Errors are the standard deviations for five values of  $|B_{max}|$ .

In conclusion, we have experimentally verified the quantum inspired optical entanglement of classical optical vortex beams having phase singularities. We have experimentally found that these classical beams violate Bell's inequality for continuous variable. The extent of violation of Bell's inequality increases with the increase in its topological charge. To obtain this, we have used the Fourier transform of two-point correlation function that provides us the Wigner distribution function of such beams. The violation of Bell's inequality in phase-space  $(x, p_x; y, p_y)$  clearly shows the existence of different spatial correlation properties for optical vortices compared to the Gaussian beam, which is similar to entanglement in quantum systems. This type of entanglement can be seen for electron vortex beams also due to the generic nature of vorticity, with far-reaching implications.

\* shaship@prl.res.in

- [1] G. Gibson, J. Courtial, M. J. Padgett, M. Vasnetsov, V. Pas'ko, S. M. Barnett, and S. Franke-Arnold, *Free-space information transfer using light beams carrying orbital angular momentum*, Opt. Express **12**, 5448 (2004).
- [2] N. Bozinovic, Y. Yue, Y. Ren, M. Tur, P. Kristensen,

- H. Huang, A. E. Willner, and S. Ramachandran, *Terabit-scale orbital angular momentum mode division multiplexing in fibers*, *Science* **340**, 1545–1548 (2013).
- [3] L. Allen, S. M. Barnett, and M. J. Padgett, *Optical angular momentum* (Institute of Physics, 2003).
- [4] L. Allen, M. Beijersbergen, R. Spreeuw, and J. Woerdman, *Orbital angular momentum of light and the transformation of laguerre-gaussian laser modes*, *Phys. Rev. A* **45**, 8185–8189 (1992).
- [5] D. G. Grier, *A revolution in optical manipulation*, *Nature* **424**, 810–816 (2003).
- [6] A. Mair, A. Vaziri, G. Weihs, and A. Zeilinger, *Entanglement of the orbital angular momentum states of photons*, *Nature* **412**, 313316 (2001).
- [7] G. Molina-Terriza, J. P. Torres, and L. Torner, *Twisted photons*, *Nat. Phys.* **3**, 305–310 (2007).
- [8] R. Horodecki, M. Horodecki, and K. Horodecki, *Quantum entanglement*, *Rev. Mod. Phys.* **81**, 865–942 (2009).
- [9] R. Fickler, R. Lapkiewicz, W. N. Plick, M. Krenn, C. Schaeff, S. Ramelow, and A. Zeilinger, *Quantum entanglement of high angular momenta*, *Science* **338**, 640–643 (2012).
- [10] B. J. McMorran, A. Agrawal, I. M. Anderson, A. A. Herzing, H. J. Lezec, J. J. McClelland, and J. Unguris, *Electron vortex beams with high quanta of orbital angular momentum*, *Science* **331**, 192–195 (2011).
- [11] J. Verbeeck, H. Tian, and P. Schattschneider, *Production and application of electron vortex beams*, *Nature* **467**, 301–304 (2010).
- [12] W. Tittel, J. Brendel, H. Zbinden, and N. Gisin, *Quantum cryptography using entangled photons in energy-time bell states*, *Phys. Rev. Lett.* **84**, 4737–4740 (2000).
- [13] A. Kumar, S. Prabhakar, P. Vaity, and R. P. Singh, *Information content of optical vortex fields*, *Opt. Lett.* **36**, 1161 (2011).
- [14] G. S. Agarwal and J. Banerji, *Spatial coherence and information entropy in optical vortex fields*, *Opt. Lett.* **27**, 800 (2002).
- [15] R. P. Singh, S. Roychowdhury, and V. Kumar Jaiswal, *Wigner distribution of an optical vortex*, *J. Mod. Opt.* **53**, 1803–1808 (2006).
- [16] M. J. Bastiaans, *The wigner distribution function applied to optical signals and systems*, *Opt. Commun.* **25**, 26–30 (1978).
- [17] P. Chowdhury, A. S. Majumdar, and G. S. Agarwal, *Nonlocal continuous-variable correlations and violation of bell’s inequality for light beams with topological singularities*, *Phys. Rev. A* **88**, 013830 (2013).
- [18] K. H. Kagalwala, G. Di Giuseppe, A. F. Abouraddy, and B. E. A. Saleh, *Bell’s measure in classical optical coherence*, *Nat. Photonics* **7**, 72–78 (2012).
- [19] C. V. S. Borges, M. Hor-Meyll, J. A. O. Huguenin, and A. Z. Khoury, *Bell-like inequality for the spin-orbit separability of a laser beam*, *Phys. Rev. A* **82**, 033833 (2010).
- [20] J. Curtis and D. Grier, *Structure of optical vortices*, *Phys. Rev. Lett.* **90**, 133901 (2003).
- [21] C. Iaconis and I. A. Walmsley, *Direct measurement of the two-point field correlation function*, *Opt. Lett.* **21**, 1783 (1996).
- [22] C.-C. Cheng, M. G. Raymer, and H. Heier, *A variable lateral-shearing sagnac interferometer with high numerical aperture for measuring the complex spatial coherence function of light*, *J. Mod. Opt.* **47**, 1237–1246 (2000).
- [23] R. Simon and G. S. Agarwal, *Wigner representation of laguerre-gaussian beams*, *Opt. Lett.* **25**, 1313 (2000).
- [24] J. S. Bell, *On the einstein-podolsky-rosen paradox*, *Physics* **1**, 195–200 (1964).
- [25] J. Clauser, M. Horne, A. Shimony, and R. Holt, *Proposed experiment to test local hidden-variable theories*, *Phys. Rev. Lett.* **23**, 880–884 (1969).
- [26] K. Banaszek and K. Wódkiewicz, *Direct probing of quantum phase space by photon counting*, *Phys. Rev. Lett.* **76**, 4344–4347 (1996).
- [27] K. Banaszek and K. Wódkiewicz, *Nonlocality of the einstein-podolsky-rosen state in the wigner representation*, *Phys. Rev. A* **58**, 4345–4347 (1998).
- [28] A. V. Carpentier, H. Michinel, J. R. Salgueiro, and D. Olivieri, *Making optical vortices with computer-generated holograms*, *Am. J. Phys.* **76**, 916 (2008).
- [29] A. Kumar, J. Banerji, and R. P. Singh, *Hanbury brown-twiss-type experiments with optical vortices and observation of modulated intensity correlation on scattering from rotating ground glass*, *Phys. Rev. A* **86**, 013825 (2012).